AMERICAN SOCIETY FOR MICROBIOLOGY | Microbiology Spectrum

RESEARCH ARTICLE

# Mechanisms and Implications of Bacterial Invasion across the Human Skin Barrier

**Zachary W. Lipsky,[a,c] Marisa Patsy,[d] Cláudia N. H. Marques,[b,c] Guy K. German[a,c]**

[a]Department of Biomedical Engineering, Binghamton University, Binghamton, New York, USA
[b]Department of Biological Sciences, Binghamton University, Binghamton, New York, USA
[c]Binghamton Biofilm Research Center, Binghamton University, Binghamton, New York, USA
[d]Fischell Department of Bioengineering, University of Maryland, College Park, Maryland, USA

**ABSTRACT** Atopic dermatitis (AD) is associated with a deficiency of skin lipids, increased populations of *Staphylococcus aureus* in the microbiome, and structural defects in the stratum corneum (SC), the outermost layer of human skin. However, the pathogenesis of AD is ambiguous, as it is unclear whether observed changes are the result of AD or contribute to the pathogenesis of the disease. Previous studies have shown that *S. aureus* is capable of permeating across isolated human SC tissue when lipids are depleted to levels consistent with AD conditions. In this study, we expand upon this discovery to determine the mechanisms and implications of bacterial penetration into the SC barrier. Specifically, we establish if bacteria are permeating intercellularly or employing a combination of both inter- and intracellular travel. The mechanical implications of bacterial invasion, lipid depletion, and media immersion are also evaluated using a newly developed, physiologically relevant, temperature-controlled drip chamber. Results reveal for the first time that *S. aureus* can be internalized by corneocytes, indicating transcellular movement through the tissue during permeation, consistent with previous theoretical models. *S. aureus* also degrades the mechanical integrity of human SC, particularly when the tissue is partially depleted of lipids. These observed mechanical changes are likely the cause of broken or ruptured tissue seen as exudative lesions in AD flares. This work further highlights the necessity of lipids in skin microbial barrier function.

**IMPORTANCE** Millions of people suffer from the chronic inflammatory skin disease atopic dermatitis (AD), whose symptoms are associated with a deficiency of skin lipids that exhibit antimicrobial functions and increased populations of the opportunistic pathogen *Staphylococcus aureus*. However, the pathogenesis of AD is ambiguous, and it remains unclear if these observed changes are merely the result of AD or contribute to the pathogenesis of the disease. In this article, we demonstrate the necessity of skin lipids in preventing *S. aureus* from penetrating the outermost barrier of human skin, thereby causing a degradation in tissue integrity. This bacterial permeation into the viable epidermis could act as an inflammatory trigger of the disease. When coupled with delipidated AD tissue conditions, bacterial permeation can also explain increased tissue fragility, potentially causing lesion formation in AD patients that results in further enhancing bacterial permeability across the stratum corneum and the development of chronic conditions.

**KEYWORDS** stratum corneum, *Staphylococcus aureus*, lipids, mechanics, atopic dermatitis, bacterial skin penetration, skin biomechanics, skin degradation

Millions of children and adults suffer from atopic dermatitis (AD) (1, 2), a chronic inflammatory skin disease. AD symptoms are associated with a deficiency of skin lipids (3), increased populations of *Staphylococcus aureus* in the microbiome (4), and structural barrier defects in the stratum corneum (SC) (5), the most superficial layer of

**Editor** Jan Claesen, Lerner Research Institute



Address correspondence to Guy K. German, ggerman@binghamton.edu.

The authors declare no conflict of interest.

**Received** 22 March 2022
**Accepted** 11 April 2022
**Published** 9 May 2022

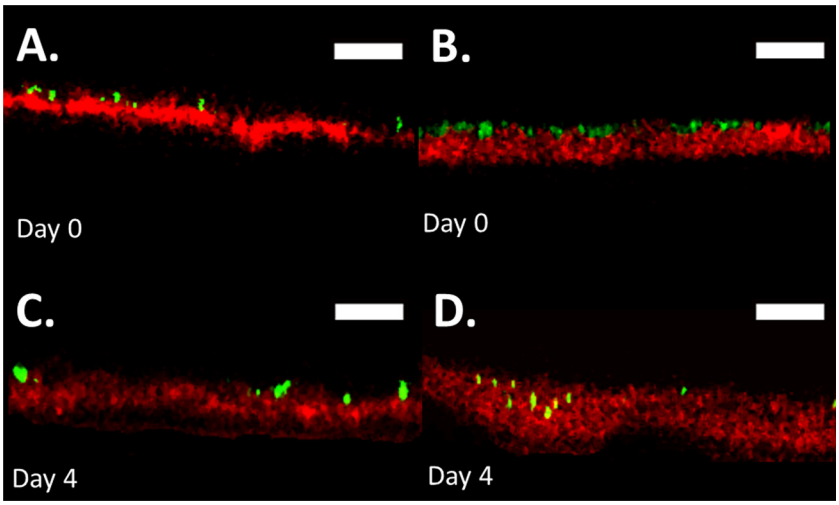


**FIG 1** *S. aureus* penetrates lipid-depleted SC in drip chamber setup. Fluorescent confocal cross-sectional profiles of *S. aureus* permeation into a control (A and C) and delipidated (B and D) SC sample over a 5-day period. Images show representative fluorescent cross-sectional profiles of BODIPY lipid-stained SC (red) inoculated with GFP-labeled *S. aureus* bacteria (green) after (A and B) 0 and (C and D) 4 days. An identical contrast change has been imposed on all images in each lipid condition to enhance visual clarity. Scale bar, 15 $\mu$m.

human skin. However, the pathogenesis of AD is ambiguous, and it is unclear if these observed changes are the result of AD or contribute to the pathology of the disease (6). We hypothesize that decreases in SC lipid populations may cause sufficient barrier dysfunction to enable *S. aureus* to permeate across the epidermis and act as a potential inflammatory trigger of the disease. This could explain the subset of cases that do not fit a genetically motivated disease development, with mutations in either immune-associated genes (interleukin 4 [IL-4], IL-13, RANTES, CD14, NOD1) (7, 8) or barrier function-associated genes (FLG) (7, 9, 10). Our previous work has shown that *S. aureus* is capable of permeating across isolated human SC tissue when lipid populations decrease to levels consistent with AD conditions (11). As an extension of this work, we aim to utilize a newly developed physiologically relevant temperature- and moisture-controlled drip chamber to investigate the pathways that allow *S. aureus* to permeate across the tissue and the mechanical and structural implications of bacterial invasion.

## RESULTS

**Lipid depletion allows permeation of *S. aureus* through the SC and internalization into corneocytes.** The ability of *S. aureus* to penetrate isolated healthy unaltered control and lipid-depleted (Delipid) human SC is first assessed. Three-dimensional bacterial penetration depths within SC samples were characterized over a 5-day period. Figure 1 shows representative composite fluorescent profile cross sections through the SC, with *S. aureus* shown in green and free fatty acids within the SC shown in red. Figure 1A and B show the position of bacteria on day 0, 2 h after inoculation, for control and lipid-depleted SC samples, respectively. Figure 1C and D show bacterial positions on day 4 for the same respective samples. Figure 1D shows that bacteria can permeate into the lipid-depleted SC, while Fig. 1C shows that bacteria on control SC do not, consistent with prior studies (11).

Interactions between bacteria and the delipidated SC tissue microstructures are further investigated to better understand permeation pathways. Previously reported models of permeation highlight that purely intercellular permeation pathways are unlikely compared with combined inter- and intracellular permeation due to permeation timescales being notably larger than those observed (11). Permeation of these nonmotile bacteria is modeled as a 3D random walk process, where the position of a new bacteria formed through binary fission is located arbitrarily next to the parent cell. For a combined inter- and intracellular permeation pathway to be viable, however, *S.*

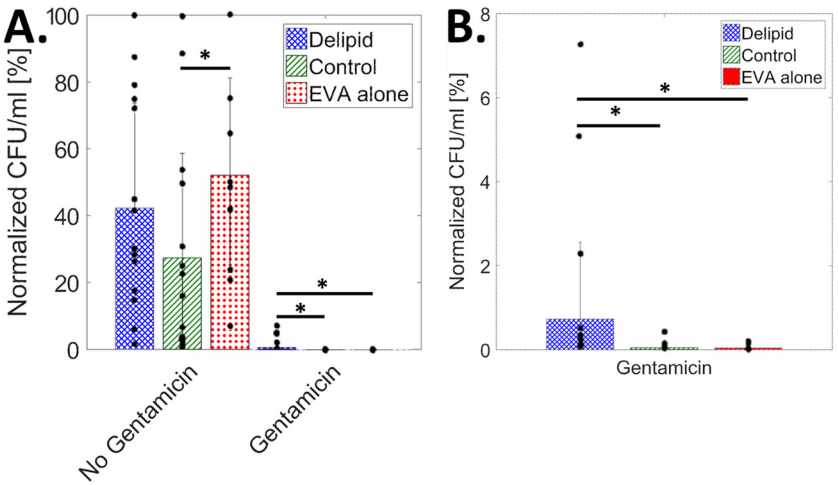


**FIG 2** *S. aureus* is internalized by corneocytes in lipid-depleted SC. (A) Average normalized bacterial population in CFU/mL, from $n = 4$ independent trials, scaled by the highest CFU/mL per trial, for delipidated SC (blue crosshatch), control SC (green stripes), and EVA alone (red dots), with and without the addition of gentamicin ($11 < n < 15$ for each condition). (B) Averaged normalized CFU/mL rescaled for gentamicin-affected conditions only. Black dots represent individual samples. Here, *, $P \leq 0.05$.

*aureus* must utilize a direct transcellular route through corneocyte cells. Internalization of *S. aureus* has previously been shown to occur both *in vivo* and *in vitro* within keratinocytes at various levels of differentiation up until the stratum granulosum (12, 13). However, internalization in anucleated corneocytes that exhibit a cornified envelope (14, 15) has not previously been observed. As such, bacterial internalization assays are next performed using methods described in Kintarak et al. (16).

Figure 2A shows the averaged ($11 \leq n \leq 15$ independent samples for each condition) *S. aureus* population in CFU/mL on delipidated and control SC samples partially embedded in an ethylene-vinyl acetate substrate (EVA) and EVA substrates alone. For each condition, populations are quantified with and without a gentamicin treatment after a 5-day growth period. Population data are normalized and scaled to the greatest CFU/mL magnitude per trial ($n = 4$). As observed previously (11, 17), the magnitude of bacteria between trials fluctuated by 36 to 68% (24 to 35% within trials). Therefore, data normalization is needed. There are no significant differences between conditions without the addition of gentamicin, except between EVA alone and control SC. As such, bacterial populations here are not statistically affected by SC lipid concentration over the 5-day timescale. As expected, bacterial population viability reduces when treated with gentamicin. Figure 2B shows a rescaled bar chart from Fig. 2A. For gentamicin-treated conditions, the reduction of bacterial population is significantly smaller in delipidated SC tissue samples, while no statistical difference exists between gentamicin-treated EVA substrates and control SC samples.

***S. aureus* alters SC mechanical properties.** We further examine the effect that *S. aureus* colonization, growth, permeation, and cellular internalization has on the mechanical properties of control and delipidated SC. To assess the independent effects of media immersion and bacterial colonization and permeation, SC samples are exposed to either *S. aureus* and media combined or media alone. These are then compared with unexposed controls. For each condition, all SC samples are equilibrated for 24 h to either 25 or 100% relative humidity (RH) prior to uniaxial testing to examine the impact of the exposure to the linear elastic and plastic regimes of the tissue. These conditions replicate environmental extremes, such as arid and wet climates, to which stratum corneum is regularly exposed (18). The isolated effect of lipid depletion is further established by comparing control and delipidated SC mechanical properties without

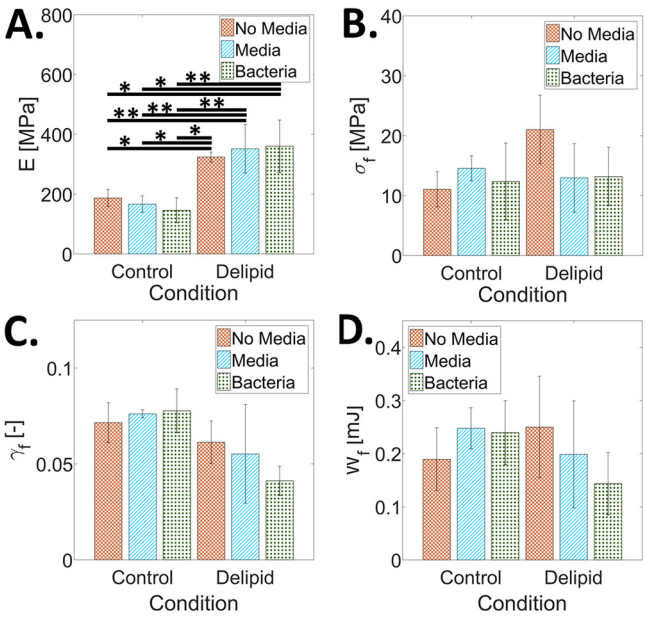


**FIG 3** The effect of *S. aureus* tissue permeation, lipid loss, and media immersion on the mechanical properties of SC equilibrated to 25% RH. Average (A) elastic modulus, $E$, (B) fractures stress, $\sigma_f$, (C) fracture strain, $\gamma_f$, and (D) work of fracture, $W_f$, for control and delipidated SC samples. Mechanical properties of SC not immersed in media are reported with orange crosshatch bars. The effect of media immersion is reported as blue striped bars. Combined media immersion and bacterial exposure effects are reported as green dotted bars. Bars denote average values of $3 \leq n \leq 8$ individual sample measurements for each treatment condition. Error bars denote standard deviations. Here, *, $P \leq 0.05$, **, $P \leq 0.01$, and ***, $P \leq 0.001$.

exposure to media, while the isolated effect of media immersion is determined for each lipid condition by comparing SC exposed to media with nonimmersed counterparts.

Figure 3 shows the average elastic modulus, $E$, fracture stress, $\sigma_f$, fracture strain, $\gamma_f$, and work of fracture, $W_f$, of control and delipidated SC subjected to the various treatment conditions and then equilibrated to 25% RH. Figure 3A shows that the elastic modulus increases only as a result of lipid depletion, consistent with previous studies (19). Neither media immersion nor bacterial growth alters the stiffness of the tissue. Figure 3B to D further highlight that at low humidity conditions, lipid depletion, media immersion, and bacteria do not have a significant effect on the fracture stress, fracture strain, or work of fracture.

Figure 4 shows complementary mechanical results for SC samples equilibrated for 24 h to 100% RH prior to mechanical testing. This conditioning enables SC tissue to undergo plastic deformation before rupture. In contrast to the 25% RH results in Fig. 3A, Fig. 4A shows that the elastic modulus does not change for delipidation alone or with media immersion of control SC. However, the elastic modulus does significantly increase with media immersion of the delipidated SC and with the addition of bacteria for both lipid conditions independently. Figure 4C similarly shows that lipid depletion alone has no significant effect on the fracture strain; however, the addition of bacteria for both lipid conditions independently causes a significant decrease in fracture strain. Figure S1 shows that the addition of bacteria for both lipid conditions decreases the ability of the SC to plastically deform. However, no significant effects are observed with the fracture strain with media immersion for either lipid condition. Figure 4B shows that fracture stress significantly increases only after lipid depletion and does not change with media immersion or the addition of bacteria for either lipid condition. Figure 4D highlights that work of fracture significantly decreases only after the combined effects of lipid depletion, media immersion, and the addition of bacteria.

**Lipid content governs crack pathways during SC rupture.** In order to better understand how delipidation and bacterial permeation induce mechanical degradation

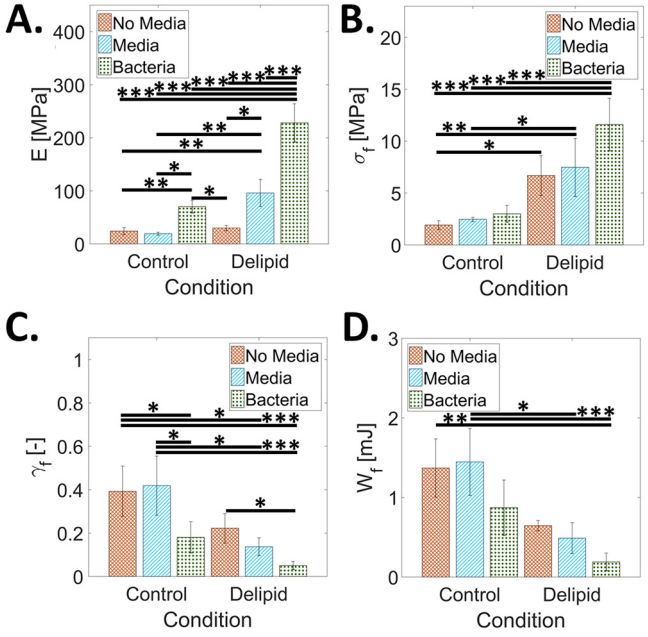


**FIG 4** The effect of *S. aureus* tissue permeation, lipid loss, and media immersion on the mechanical properties of SC at 100% RH. Average (A) elastic modulus, $E$, (B) fractures stress, $\sigma_f$, (C) fracture strain, $\gamma_f$, and (D) work of fracture, $W_f$, for control and delipidated SC samples. Mechanical properties of SC not immersed in media are reported with orange crosshatch bars. The effect of media immersion is reported as blue striped bars. Combined media immersion and bacterial exposure effects are reported as green dotted bars. Bars denote average values of $3 \leq n \leq 8$ individual sample measurements for each treatment condition. Error bars denote standard deviations. Here, *, $P \leq 0.05$, **, $P \leq 0.01$, and ***, $P \leq 0.001$.

of SC, along with what constituent components of the structurally heterogeneous tissue are affected at the microscale, tissue fractography studies are performed. Here, the impact of lipid depletion, media immersion, and bacterial permeation on changes to the failure pathways that form during SC rupture are quantified. Widefield histological imaging (Fig. 5A to D) and scanning electron microcopy (SEM) (Fig. 5E to H) are used to identify intact corneocyte cell edges along the failure pathway. Similar failure pathways are observed at both low- and high-humidity conditions, as well as with and without immersion for each independent lipid condition. Using histological images in Fig. 5A to D, the proportion of the failure pathway coincident with corneocyte cell

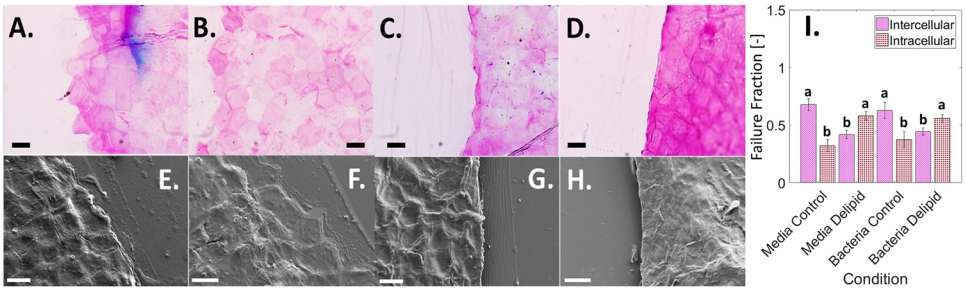


**FIG 5** Effect of lipids and bacteria on SC failure pathway. (A to D) Brightfield images of SC crack pathways using TBBF stain to highlight polygonal shaped corneocytes. (E to H) SEM images of SC crack pathways. Scale bars, 30 $\mu$m. Conditions tested include control SC exposed to media only (A and E), control SC exposed to media and bacteria (B and F), delipidated SC exposed to media only (C and G), and delipidated SC exposed to media and bacteria (D and H). (I) Average percentage of total inter- (purple crosshatch) and intra- (red dots) cellular failure, normalized by total SC crack length for different lipid and exposure conditions. Bars denote average values from $n = 114 \pm 5$ individual corneocytes from $n = 3$ SC samples for each lipid and exposure condition. Error bars denote standard deviations. "a" and "b" in the figure independently denote bars that are not statistically different from one another but are statistically different to the contrasting letter with a minimum of $P < 0.05$.

edges (intercellular failure) or ruptured cells (intracellular failure) is summed and normalized by the total failure path length. Averaged values for each condition, as shown in Fig. 5I, reveal that intercellular failure is statistically predominant for control SC conditions, while intracellular failure is significantly greater for delipidated conditions, regardless of bacterial or media exposure.

## DISCUSSION

Previous studies have shown that *S. aureus* can permeate into and across partially delipidated SC, with bacteria located within the tissue by day 6 of flow cell incubation at room temperature (23°C) and full permeation by day 9 (11). Using a more physiologically relevant drip chamber arrangement that more closely mimics skin temperature and diurnal hydration/dehydration cycles, we find that permeation into the tissue occurs more rapidly. Figure 1D shows bacterial penetration into SC by day 4. We speculate that the accelerated rate of penetration is related to the increased temperature (23 to 33°C), which more accurately represents the average skin surface temperature (20, 21). The lack of inversion used in the flow cell setup may also increase permeation rates, due to increased initial bacterial sedimentation on the skin. Further, the bacterial presence within corneocytes only under delipidated SC conditions, as shown in Fig. 2, confirms bacterial permeation via intra- and intercellular pathways, further supporting a previously published diffusion model (11) that predicts that bacteria are more likely to take a direct transcellular permeation route rather than a purely intercellular pathway. Previous literature has reported the internalization of *S. aureus* into other nonprofessional phagocytes, including osteoblasts (22–24), keratinocytes (16, 25, 26), and endothelial cells (27–29). When comparing the similarity in normalized CFU/mL for gentamicin-treated tissue, there is increased viability in the delipidated case relative to the EVA alone and control SC, indicating that bacterial internalization can occur in corneocytes but only when the tissue is partially delipidated.

We additionally investigate the effects that bacterial colonization, penetration, and bacterial internalization have on the mechanical properties of the SC under control and partially lipid-depleted conditions. At high RH, delipidation alone increases only the fracture stress. However, for both lipid conditions, we observe an increase in tissue elastic modulus and a decrease in the ability to plastically deform with bacterial exposure (Fig. 4A and C, respectively). These changes increase the risk of fracture within physiologically relevant strains and result in a degradation of the mechanical integrity of the tissue (Fig. 4D). A similar trend occurs with a reduction in SC water content (30–34). Previous studies report changes in the water-holding capacity of SC with loss of extracellular lipid (35), natural moisturizing factor (NMF) depletion (36), and hyaluronan levels (37). So, while changes in the water-holding capacity would explain alterations in the elastic modulus of tissue due to delipidation (Fig. 3A), additional bacterial permeation may consequently also be affecting the presence of extracellular lipids (38–43), NMFs (44–47), and hyaluronan (48–50) that would affect the water retention ability of the tissue, potentially caused by a disruption of cornified envelopes during bacterial invasion into the corneocyte cells. Comparing the effect of bacterial permeation, immersion, and delipidation on the elastic modulus of the SC at low RH conditions in Fig. 3A, we observe that only lipid depletion (51–55) causes a significant change in the elastic modulus of the tissue. Neither media immersion, associated with a loss of NMFs (43, 47, 56–58), nor bacterial presence affects tissue stiffness for either lipid condition.

In addition to investigating the mechanical properties of SC tissue, the impact of lipid depletion, media immersion, and bacterial growth on changes to the microstructural mechanical integrity are also quantified. When observing fracture path in control and delipidated SC tissue (Fig. 5), cracking occurs intercellularly for the control conditions yet intracellularly for the delipidated conditions, irrespective of media immersion or bacteria growth (Fig. 5I). We anticipate that this lipid depletion induced a change in the way cells rupture occurs due to the formation of strong interactions between adjacent lipid envelopes in intercellular regions of SC (59), resulting in an energetically less

favorable failure between corneocytes and a preference for rupture of the keratin intermediate filament network within corneocytes, observable in Fig. 4B. While this change in the type of cellular failure is not directly caused by bacterial invasion into the tissue, the depletion of lipids that causes this change, however, is associated with the partially delipidated skin state with atopic dermatitis.

*S. aureus* does not produce any ceramidase (60), nor has this bacterial species previously been shown to alter stratum corneum lipids directly. Nonetheless, the impact of bacterial growth and permeation on skin shows changes in the mechanical properties of SC consistent with lipid depletion: a stiffening and weakening of the tissue. This seems, therefore, to suggest that the bacteria may potentially be altering other components of the tissue. The most likely alternative is that bacteria are affecting NMFs and/or hyaluronan, either directly through enzyme degradation or indirectly, for NMFs, by leaching out of the cornified envelope during cellular internalization. Certainly, the most prominent NMFs, urocanic acid (UCA) (61), Ser (62), pyrrolidine carboxylic acid (PCA) (63), glycerol (64), and urea (65), as well as hyaluronan (66), have all been shown to be affected directly by *S. aureus*. To ascertain the cause of bacterial medicated tissue degradation, NMF and hyaluronan levels in SC tissue inoculated with bacteria should be compared with unexposed controls, for both normal and lipid-depleted conditions, possibly using HPLC (67). It should be noted that while keratin filaments have been hypothesized to plasticize with the addition of water at high RH, contributing to SC viscoelastic properties (30, 68, 69), there have been no studies, to our knowledge, looking into the isolated mechanical effect of keratin modification in SC or the effect that *S. aureus* has on keratin in skin corneocytes. Moreover, these assessments should also be investigated in future studies.

**Conclusion.** In this article, the ability of *Staphylococcus aureus* to become internalized by corneocytes in lipid-depleted human stratum corneum during permeation is shown. This ability indicates that a transcellular permeation route through the tissue is viable. The impact of changes in lipid composition, immersion, and bacterial growth into and across stratum corneum on the mechanical degradation of the tissue are also revealed. Bacterial growth acts to weaken the tissue and make it more brittle, increasing the risk of tissue rupture. Skin suffering from atopic dermatitis is associated with depleted levels of lipids (70) and increased populations of *S. aureus* bacteria in the microbiome (17, 71). Lipid depletion and bacterial mediated mechanical degradation of the tissue could further explain the formation of exudative lesions associated with atopic dermatitis. These regions of ruptured tissue would lead to further entry of bacteria and other allergens into the viable epidermis, contributing to a chronic state of the disease. In addition, this work shows the necessity of lipids in not only preventing bacterial entry into the skin but also governing stratum corneum mechanical barrier integrity and fracture behavior. This is especially important for people that might be prone to lipid depletion through abnormalities in lipid-processing proteins (72), occupational hazards such as repeated hand washing required for sterile environments (73, 74), or contact with metal working fluids, solvents, and caustic chemicals (75). Last, the connection between bacteria and immersion (natural moisturizing factors) could contribute to a lack of natural moisturizing factors observed in the stratum corneum of atopic dermatitis patients (76, 77).

## MATERIALS AND METHODS

**Bacterial strains.** All bacterial studies used *Staphylococcus aureus* ATCC 6538 (Rosenbach, American Type Culture Collection [ATCC], Manassas, VA) isolated from human lesions. This strain was modified with *pALC2084* and edited to constitutively express green fluorescence protein (GFP) (11, 17). Overnight cultures were grown in brain heart infusion medium (BHI; Becton, Dickinson, Sparks, MD) supplemented with 10 mg/L chloramphenicol (Mediatech, Corning Life Sciences, Corning, NY) for plasmid maintenance and 250 ng/mL tetracycline (Amresco, Solon, OH) for induction of GFP, in Erlenmeyer flasks at 37°C with agitation (220 rpm).

**Stratum corneum isolation.** A full-thickness (76 years) female cadaveric abdominal skin sample was obtained from ConnectLife (Syracuse, NY). In accordance with the Department of Health and Human Services regulations, 45 CFR 46.101:b:4, an exempt approval (3002-13) was attained to perform research using deidentified tissue samples. SC was isolated using standard heat bath and trypsin techniques (78).

After isolation, SC sheets were placed on plastic mesh, rinsed in deionized water (DIW), and dried at room temperature and RH (23 ± 2°C, 29% ± 3% RH).

**Stratum corneum lipid depletion.** SC sheets were divided equally into two groups: (i) a control group immersed in DIW for 60 min (this treatment does not deplete lipids or irreversibly alter the intercellular lipid structure) (79) and (ii) a treatment group, immersed in a 2:1 mixture of chloroform and methanol (Sigma-Aldrich, St. Louis, MO) for 60 min, partially depleting intercellular ceramide, cholesterol, and free fatty acid lipids found in SC from the tissue (11, 17, 33, 55, 80). From estimates of human SC lipid concentrations and composition (52, 81, 82), treatments using similar solvent extraction protocols on human and porcine SC (51–54) reduce lipids by 54% ± 30%. SC samples were then punched out from both control and lipid-depleted (Delipid) SC tissue sheets with either a circular 6-mm diameter punch (Harris Uni-Core, Redding, CA) for the internalization assay ($n = 30$ control; $n = 30$ delipid) or a rectangular 9.53 by 19.05 mm punch (SYNEO, Angleton, TX) for mechanical testing ($n = 26$ control; $n = 26$ delipid).

**Substrate preparation for mechanical testing.** A 20% wt/vol ethylene-vinyl acetate (EVA) in toluene was prepared and spin coated (WS-400B-6NNP/LITE, Laurell Technologies Corporation, North Wales, PA) onto a glass coverslip (25 by 75 mm, Electron Microscopy Sciences, Hatfield, PA) at 50 rpm for 20 s. After evaporation of toluene for 12 h, this produced a uniform EVA film with a thickness of 91 ± 17 $\mu$m. EVA substrates were then placed on a hotplate (10027-028, VWR, Radnor, PA) at 60°C to allow the EVA to soften for SC sample attachment. This temperature has been shown not to create irreversible changes to the structural properties of SC (83). Control and delipidated SC samples were then alternately embedded along the long axis of the cover slip ($n = 6$ samples arranged in a 3 by 2 grid on each substrate), leaving only their outermost face exposed. This embedding process occludes the sides and underside of the SC sample, preventing bacterial growth in these regions. For each substrate tested, the order of the conditioned SC samples deposited was randomized. Substrates were then degassed in a vacuum desiccator (5310-0250, Nalgene, ThermoFisher Scientific, Waltham, MA) with attached vacuum pump (ME4 NT Vacuubrand, BrandTech, Essex, CT) for 4 h. This process eliminated microbubbles between the SC and EVA.

**Drip chamber setup and inoculation.** Embedded SC substrates were sterilized under germicidal UV light (254 nm) for 15 min and then mounted in the custom-built drip chamber (Fig. S2). This UV treatment does not alter the mechanical properties of the tissue (84). The drip chamber is an aluminum hollow block (10 by 112 by 34 mm) that has eight samarium-cobalt magnets (M14X116DISmCo, Apex Magnets, Petersburg, WV) at each corner of the underside and top. Substrates with embedded SC samples were sandwiched between the bottom steel plate and the block's magnets, holding the substrate in place magnetically. Vacuum grease (Dow Corning, Midland, Michigan) was also applied around the edges of the substrate to ensure that the drip chamber was fully sealed. The upper steel plate holds another glass cover slip in place magnetically. This upper plate and cover slip could be slid backwards to allow for the addition of medium over the SC surface. The shorter sides of the block have threaded holes for a brass inlet (5454K62, McMaster-Carr, Chicago, IL) and outlet. The brass inlet was connected to a gas permeable filter (200 nm pore size) via silicone tubing (96400-14, Cole-Parmer, Vernon Hills, IL) to maintain atmospheric pressure. The brass outlet was connected to a cross connector (5463K93, McMaster-Carr, Chicago, IL) via silicone tubing. The cross connector separates the injection ports for the fatty acid dye (D3835, ThermoFisher Scientific, Waltham, MA) and bacterial inoculum and an outlet port for waste. Each port on the cross connecter was connected to a luer lock coupling (51525K322, McMaster-Carr, Chicago, IL) via silicone tubing. The drip chamber was first injected with 5 mL fatty acid dye at a 10 $\mu$M concentration in 10% BHI medium (Franklin Lakes, NJ). The lipid stain was allowed to bind to all SC samples for 30 min. To remove unbound dye from the chamber, 15 mL phosphate-buffered saline (PBS) was injected into the chamber and then decanted out of the outlet port. The fluorescent fatty acid stain was found not to alter the growth behavior of the bacteria. Following staining, the chamber was injected with 5 mL of a stationary-phase culture of *S. aureus* ($10^8$ CFU/mL). The bacteria were allowed to attach to the SC surface for 2 h. Unattached bacteria were washed away with 15 mL of PBS, injected into the chamber, and then decanted. The top of the drip chamber was then slid backwards and 2 drops (50 $\mu$L/drop) of 20% BHI medium, supplemented with 250 ng/mL tetracycline for induction of GFP, was added to each SC sample to maintain hydration and bacterial growth. The top was then slid back into place, and the chamber was placed on a hotplate (10027-028, VWR, Radnor, PA) to simulate average skin surface temperature at 33°C (20, 21). Medium was added to the chamber each day for 5 days total until sterilization and removal of the SC from the substrate for mechanical testing. The setup was kept in a biosafety level 2 hood (class II type A2, Labconco, Kansas City, MO), except for imaging.

**Microscopic imaging of bacterial colonization of SC.** *S. aureus* growth was monitored every 24 h using confocal laser scanning microscopy (Leica SP5, Wetzlar, Germany) over a 5-day period. Images with a spatial resolution of 0.38 $\mu$m/pixel (1,024 by 1,024 pixels) were acquired using a 40× lens objective with a numerical aperture of 1.25. SC samples were illuminated sequentially with transmitted light and then at 455 and 543 nm. Images for the latter two excitation wavelengths were captured, respectively, across a bandwidth of 500 to 540 and 560 to 590 nm. Transmitted light images were used to distinguish topographical regions of the SC to enable consistent imaging of the same position every day, to within ~5 $\mu$m spatial accuracy. The SC position imaged was carefully chosen as to not include voids in the SC tissue arising from apocrine pores (11). The 455 nm illumination was used to excite GFP-tagged *S. aureus*. The 543 nm illumination was used to excite the fluorescent BODIPY stained SC. At each recorded time point, z-stack images were taken across the full depth of the SC sample and substrate at height increments of 0.15 $\mu$m.

**Internalization assay.** Individual wells in 24-well plates ($n = 4$ plates total) were coated with 200 $\mu$L of 20% EVA polymer dissolved in toluene. The solvent was then allowed to evaporate for 12 h. Control

($n = 8$) and delipid ($n = 8$) SC samples were then independently embedded in each well, leaving only their outermost face exposed. Wells containing EVA alone ($n = 8$) were used as tissue-free controls. Each 24-well plate was then degassed in a vacuum desiccator for 4 h to eliminate microbubbles between the SC and EVA. The well plates were then sterilized under UV light for 15 min. Following this, each well was filled with 300 $\mu$L stationary-phase culture of *S. aureus* ($10^8$ CFU/mL). The bacteria were allowed to attach to the SC surface or EVA polymer alone for 2 h. Unattached bacteria were washed away with three rinses of PBS. Each day thereafter, for 5 days, 2 drops (50 $\mu$L/drop) of 20% BHI medium, supplemented with 250 ng/mL tetracycline, were added to each well to maintain hydration and bacterial growth. Plates were then placed on a hotplate at 33°C. On the 5th day, methods described in Kintarak et al. were used (16). Half of the wells under each condition (control, delipidated, EVA alone) were exposed to a 1 mL solution of 100 $\mu$g/mL of gentamicin, killing extracellular bacteria. The plate was then incubated for 2 h at 37°C and rinsed twice with PBS. Each well was then filled with 1 mL 0.5% Triton X-100 (Sigma-Aldrich, St. Louis, MO). Wells containing SC were macerated with a pipette tip. To determine internalized bacterial viable counts, serial dilutions of each well were plated on 2:1 plate count agar (247930, BD, Franklin Lakes, NJ) to standard agar (214530, BD, Franklin Lakes, NJ).

**SC sterilization, removal, and mechanical testing.** After 5 days of bacterial colonization and subsequent permeation, substrates were sterilized with a 2.5 mL/L aqueous bleach solution (Clorox, Oakland, CA) in DIW for 30 min (85–87). After sterilization, substrates were placed in a water bath at 60°C for 5 min to soften the EVA and dislodge the SC rectangles for subsequent mechanical testing. Figure S3 shows that this concentration of bleach solution did not cause significant changes in SC mechanical properties. SC samples were then equilibrated for 24 h to either 25% or 100% RH before mechanical testing ($3 \leq n \leq 8$ independent samples for each lipid condition and humidity). Equilibration to low or high RH conditions was achieved by placing specimens, respectively, in an airtight container filled with desiccant (Drierite 10 to 20 mesh, W.A. Hammond Drierite Company, Xenia, OH) or a hydration cabinet (F42072-1000, Secador, Wayne, NJ) with a base filled with DIW. In both cases, RH conditions were monitored throughout the equilibration period using a hygrometer with probe (445815, Extech Instruments, Nashua, NH)). After equilibration, the mechanical properties of samples were evaluated using a uniaxial tensometer (UStretch, CellScale, Waterloo, ON, Canada) equipped with a 4.4 N load cell. The ends of each SC sample were taped (General-Purpose Laboratory Labeling Tape, VWR, Radnor, PA) to prevent slippage of the sample in the tensometer grips, leaving an exposed area of 9.53 by 10 mm. Individual SC samples were mounted into opposing tensometer grips, initially separated by 10 mm. Samples were strained until rupture at a constant strain rate of 0.012 $s^{-1}$, similar to rates used in previous mechanical studies of skin (88). Tensile forces and grip separation were recorded at a frequency of 5 Hz. After mechanical testing, the average thickness of the ruptured SC sample was quantified with optical microscopy using an Eclipse Ti-U inverted microscope (Nikon, Melville, NY) with 40× oil lens objective (Nikon Plan UW, Nikon, Melville, NY). Images were recorded using a digital CCD camera (Andor Clara, Belfast, Northern Ireland). Optical thickness measurements were taken a distance from the crack interface to prevent measuring reduced thicknesses arising from plastic deformation. Combinations of sample dimensions and recorded force-displacement data were then used to derive engineering stress-strain curves, from which the average elastic modulus, fracture stress, fracture strain, and work of fracture were extracted. SC subjected to the same protocol without the addition of bacteria was used as the media control for each lipid condition.

**SC failure pathway imaging and failure method calculation.** After mechanical testing, fractured SC sample pieces were subjected to either SEM ($n = 3$ sample halves per condition) or histological staining and widefield transmission microscopy ($n = 3$ sample halves per condition) to determine the proportion of inter- and intracellular crack pathways. For SEM imaging, fractured halves were laminated onto square glass coverslips (22 X22X-2, Thermofisher Scientific, Waltham, MA) and adhered to SEM pin mounts (16144, TED PELLA, Redding, CA) using carbon tape (16084-3, TED PELLA, Redding, CA). To increase conduction, copper tape (102091-345, VWR, Radnor, PA) was used to create a path from the bottom of the chuck to the fractured SC sample. The SEM substrate was then sputtered using a carbon coater (208C high vacuum turbo carbon coater, Cressington). SC failure pathways were then imaged on an SEM (ZEISS FEG- SEM Supra 55 VP) with a voltage of 0.7 to 1.5 kV. For histological staining, fractured halves were laminated onto glass slides (16004-422, VWR, Radnor, PA) and exposed to toluidine blue and basic fuchsin (TBBF) stain in 30% ethanol (Delasco, Council Bluffs, IA) for 1 min. This process dyes the intercellular regions of the SC, enabling visualization of individual corneocytes. Slides were then rinsed with DIW for 1 min and allowed to dry for 2 h. A drop of mounting medium (8310-16, Thermofisher Scientific, Waltham, MA) was then added to each slide before the coverslip was mounted (48393-059, VWR, Radnor, PA). Prepared slides were then imaged along the failure pathway using a light microscope (BX43, Olympus, Tokyo, Japan) and 50× objective.

Images of the SC failure pathway from the TBBF-stained tissue samples were used to quantify the total fracture crack length and the proportions of both intercellular (Fig. 6A) and intracellular failure (Fig. 6B). Intercellular failure resulted in intact corneocytes with well-defined polygonal edges. Intracellular failure resulted in broken corneocytes without well-defined polygonal morphologies. Images were taken interspersed across the entire width of the SC sample (9.53 mm), representing 13 to 21% of the total crack length ($n = 3$ samples per condition, $n = 114 \pm 5$ corneocytes total per condition). Corneocytes with edges that were not all well distinguished were not used, as shown in Fig. 6C. The total lengths of intercellular and intracellular failure normalized by the total crack length measured provide the proportion of intercellular to intracellular failure for each condition.

**Statistical analysis.** All statistical analyses were performed using R (version 3.4.2). A 1-way analysis of variance (ANOVA) was used to test for statistical significance in Fig. 2, where the addition or lack of

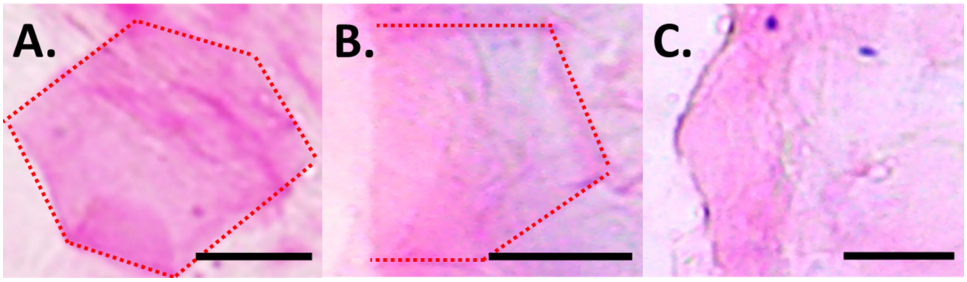


**FIG 6** Corneocyte integrity along SC failure pathway. Examples of TBBF-stained (A) intact, (B) broken, and (C) indistinguishable corneocytes imaged at 50× along a fractured SC pathway. Scale bar, 15 $\mu$m.

gentamicin was compared independently across all sample types (Control, Delipid, and EVA alone), Fig. 3 and 4, where comparisons were made across all lipid and exposure conditions, and Fig. 5I, where comparisons were made across all failure preferences and lipid and exposure conditions. Levene's and Shapiro-Wilk's tests were, respectively, used to determine equality of variances and normality. Results in Fig. 2A and B were found to exhibit nonnormal distributions and unequal variance. Here, a Kruskal-Wallace analysis was performed. Results in Fig. 3A and Fig. 4B and C were found to exhibit normal distributions and unequal variances. Here, a 1-way ANOVA with Welch correction was performed. Results in Fig. 3B to D, Fig. 4A and D, and Fig. 5I were found to exhibit normal distributions and equal variances. Here, a standard 1-way ANOVA was performed. *Post hoc* analyses were performed if statistical significance levels below 5% were established. In the figures, *, $P \leq 0.05$, **, $P \leq 0.01$, ***, $P \leq 0.001$, and matching letters indicates $P \geq 0.05$.

## SUPPLEMENTAL MATERIAL

Supplemental material is available online only.

**SUPPLEMENTAL FILE 1**, PDF file, 0.4 MB.

## ACKNOWLEDGMENTS

This material is based upon work supported by the National Science Foundation under grant no. 1653071 and grant no. 1757846. We also thank Elana Chazen, Amanda Kenny, and Caitlin M Begley for originally designing the drip chamber device. We also thank F.D.C. Willard for useful conversations about this work.

We declare no conflict of interest.

## REFERENCES

1. Barbarot S, Auziere S, Gadkari A, Girolomoni G, Puig L, Simpson EL, Margolis DJ, Bruin-Weller M, Eckert L. 2018. Epidemiology of atopic dermatitis in adults: results from an international survey. Allergy Eur J Allergy Clin Immunol 73:1284–1293. https://doi.org/10.1111/all.13401.
2. Asher MI, Montefort S, Björkstén B, Lai CK, Strachan DP, Weiland SK, Williams H. 2006. Worldwide time trends in the prevalence of symptoms of asthma, allergic rhinoconjunctivitis, and eczema in childhood: ISAAC phases one and three repeat multicountry cross-sectional surveys. Lancet 368:733–743. https://doi.org/10.1016/S0140-6736(06)69283-0.
3. Imokawa G, Abe A, Jin K, Higaki Y, Kawashima M, Hidano A, Imokawa GL of C in SC of ADAEF in ADS. 1991. Decreased level of ceramides in stratum corneum of atopic dermatitis: an etiologic factor in atopic dry skin? J Invest Dermatol 96:523–526. https://doi.org/10.1111/1523-1747.ep12470233.
4. Chiller K, Selkin BA, Murakawa GJ. 2001. Skin microflora and bacterial infections of the skin. J Invest Dermatol Symp Proc 6:170–174. https://doi.org/10.1046/j.0022-202x.2001.00043.x.
5. Agrawal R, Woodfolk JA. 2014. Skin barrier defects in atopic dermatitis. Curr Allergy Asthma Rep 14:433. https://doi.org/10.1007/s11882-014-0433-9.
6. Sullivan M, Silverberg NB. 2017. Current and emerging concepts in atopic dermatitis pathogenesis. Clin Dermatol 35:349–353. https://doi.org/10.1016/j.clindermatol.2017.03.006.
7. Barnes KC. 2010. An update on the genetics of atopic dermatitis: scratching the surface in 2009. J Allergy Clin Immunol 125:16–29.e1-11. https://doi.org/10.1016/j.jaci.2009.11.008.
8. Hanifin JM. 2009. Evolving concepts of pathogenesis in atopic dermatitis and other eczemas. J Invest Dermatol 129:320–322. https://doi.org/10.1038/jid.2008.252.
9. Morar N, Cookson WOCM, Harper JI, Moffatt MF. 2007. Filaggrin mutations in children with severe atopic dermatitis. J Invest Dermatol 127:1667–1672. https://doi.org/10.1038/sj.jid.5700739.
10. Palmer CNA, Irvine AD, Terron-Kwiatkowski A, Zhao Y, Liao H, Lee SP, Goudie DR, Sandilands A, Campbell LE, Smith FJD, O'Regan GM, Watson RM, Cecil JE, Bale SJ, Compton JG, DiGiovanna JJ, Fleckman P, Lewis-Jones S, Arseculeratne G, Sergeant A, Munro CS, El Houate B, McElreavey K, Halkjaer LB, Bisgaard H, Mukhopadhyay S, McLean WHI. 2006. Common loss-of-function variants of the epidermal barrier protein filaggrin are a major predisposing factor for atopic dermatitis. Nat Genet 38:441–446. https://doi.org/10.1038/ng1767.
11. Lipsky ZW, Marques CNH, German GK. 2020. Lipid depletion enables permeation of Staphylococcus aureus bacteria through human stratum corneum. Tissue Barriers 8:1754706. https://doi.org/10.1080/21688370.2020.1754706.
12. Soong G, Paulino F, Wachtel S, Parker D, Wickersham M, Zhang D, Brown A, Lauren C, Dowd M, West E, Horst B, Planet P, Prince A. 2015. Methicillin-resistant Staphylococcus aureus adaptation to human keratinocytes. mBio 6. https://doi.org/10.1128/mBio.00289-15.
13. Rigaill J, Morgene MF, Gavid M, Lelonge Y, He Z, Carricajo A, Grattard F, Pozzetto B, Berthelot P, Botelho-Nevers E, Verhoeven PO. 2018. Intracellular activity of antimicrobial compounds used for Staphylococcus aureus nasal decolonization. J Antimicrob Chemother 3:3044–3048. https://doi.org/10.1093/jac/dky318.
14. Candi E, Schmidt R, Melino G. 2005. The cornified envelope: a model of cell death in the skin. Nat Rev Mol Cell Biol 6:328–340. https://doi.org/10.1038/nrm1619.

15. Kalinin A, Marekov LN, Steinert PM. 2001. Assembly of the epidermal cornified cell envelope. J Cell Sci 114:3069–3070. https://doi.org/10.1242/jcs.114.17.3069.
16. Kintarak S, Whawell SA, Speight PM, Packer S, Nair SP. 2004. Internalization of Staphylococcus aureus by human keratinocytes. Infect Immun 72:5668–5675. https://doi.org/10.1128/IAI.72.10.5668-5675.2004.
17. Cleary JM, Lipsky ZW, Kim M, Marques CNH, German GK. 2018. Heterogeneous ceramide distributions alter spatially resolved growth of Staphylococcus aureus on human stratum corneum. J R Soc Interface 15:20170848. https://doi.org/10.1098/rsif.2017.0848.
18. Shoenfeld Y, Sohar E, Ohry A, Shapiro Y. 1976. Heat stress: comparison of short exposure to severe dry and wet heat in saunas. Arch Phys Med Rehabil.
19. German GKK, Pashkovski E, Dufresne ERR. 2013. Surfactant treatments influence drying mechanics in human stratum corneum. J Biomech 46:2145–2151. https://doi.org/10.1016/j.jbiomech.2013.07.003.
20. Winkel J, Jørgensen K. 1991. Significance of skin temperature changes in surface electromyography. Eur J Appl Physiol 63:345–348. https://doi.org/10.1007/BF00364460.
21. Atmaca I, Yigit A. 2006. Predicting the effect of relative humidity on skin temperature and skin wettedness. J Therm Biol 31:442–452. https://doi.org/10.1016/j.jtherbio.2006.03.003.
22. Van Nhieu GT, Isberg RR. 1993. Bacterial internalization mediated by $\beta$1 chain integrins is determined by ligand affinity and receptor density. EMBO J 12:1887–1895. https://doi.org/10.1002/j.1460-2075.1993.tb05837.x.
23. Sinha B, Francois PP, Nusse O, Foti M, Hartford OM, Vaudaux P, Foster TJ, Lew DP, Herrmann M, Krause K-H. 1999. Fibronectin-binding protein acts as Staphylococcus aureus invasin via fibronectin bridging to integrin $\alpha5\beta1$. Cell Microbiol 1:101–117. https://doi.org/10.1046/j.1462-5822.1999.00011.x.
24. Fowler T, Wann ER, Joh D, Johansson S, Foster TJ, Höök M. 2000. Cellular invasion by Staphylococcus aureus involves a fibronectin bridge between the bacterial fibronectic-binding MSCRAMMs and host cell $\beta$1 integrins. Eur J Cell Biol 79:672–679. https://doi.org/10.1078/0171-9335-00104.
25. Dziewanowska K, Carson AR, Patti JM, Deobald CF, Bayles KW, Bohach GA. 2000. Staphylococcal fibronectin binding protein interacts with heat shock protein 60 and integrins: role in internalization by epithelial cells. Infect Immun 68:6321–6328. https://doi.org/10.1128/IAI.68.11.6321-6328.2000.
26. Hirschhausen N, Schlesier T, Schmidt MA, Götz F, Peters G, Heilmann C. 2010. A novel staphylococcal internalization mechanism involves the major autolysin Atl and heat shock cognate protein Hsc70 as host cell receptor. Cell Microbiol 12:1746–1764. https://doi.org/10.1111/j.1462-5822.2010.01506.x.
27. Askarian F, Uchiyama S, Valderrama JA, Ajayi C, Sollid JUE, van Sorge NM, Nizet V, van Strijp JAG, Johannessen M. 2017. Serineaspartate repeat protein D increases Staphylococcus aureus virulence and survival in blood. Infect Immun 85. https://doi.org/10.1128/IAI.00559-16.
28. McDonnell CJ, Garciarena CD, Watkin RL, McHale TM, McLoughlin A, Claes J, Verhamme P, Cummins PM, Kerrigan SW. 2016. Inhibition of major integrin $\alpha$V$\beta$3 reduces Staphylococcus aureus attachment to sheared human endothelial cells. J Thromb Haemost 14:2536–2547. https://doi.org/10.1111/jth.13501.
29. Claes J, Liesenborghs L, Peetermans M, Veloso TR, Missiakas D, Schneewind O, Mancini S, Entenza JM, Hoylaerts MF, Heying R, Verhamme P, Vanassche T. 2017. Clumping factor A, von Willebrand factor-binding protein and von Willebrand factor anchor Staphylococcus aureus to the vessel wall. J Thromb Haemost 15:1009–1019. https://doi.org/10.1111/jth.13653.
30. Papir Y, Hsu K, Wildnauer RH, Hsh K, Wildnauer RH, Hsu K, Wildnauer RH. 1975. The mechanical properties of stratum corneum: I. The effect of water and ambient temperature on the tensile properties of newborn rat stratum corneum. Biochim Biophys Acta (BBA) – General Subjects 399:170–180. https://doi.org/10.1016/0304-4165(75)90223-8.
31. Alonso A, Meirelles NC, Yushmanov VE, Tabak M. 1996. Water increases the fluidity of intercellular membranes of stratum corneum: correlation with water permeability, elastic, and electrical resistance properties. J Invest Dermatol 106:1058–1063. https://doi.org/10.1111/1523-1747.ep12338682.
32. Wildnauer RH, Bothwell JW, Douglass AB. 1971. Stratum corneum biomechanical properties I. Influence of relative humidity on normal and extracted human stratum corneum. J Invest Dermatol 56:72–78. https://doi.org/10.1111/1523-1747.ep12292018.
33. Liu X, Cleary J, German GK. 2016. The global mechanical properties and multi-scale failure mechanics of heterogeneous human stratum corneum. Acta Biomater 43:78–87. https://doi.org/10.1016/j.actbio.2016.07.028.
34. Wu KS, van Osdol WW, Dauskardt RH. 2006. Mechanical properties of human stratum corneum: effects of temperature, hydration, and chemical treatment. Biomaterials 27:785–795. https://doi.org/10.1016/j.biomaterials.2005.06.019.
35. Imokawa G, Hattori M. 1985. A possible function of structural lipids in the water-holding properties of the stratum corneum. J Invest Dermatol 84:282–284. https://doi.org/10.1111/1523-1747.ep12265365.
36. Visscher MO, Tolia GT, Wickett RR, Hoath SB. 2003. Effect of soaking and natural moisturizing factor on stratum corneum water-handling properties. J Cosmet Sci 54:289–300.
37. Witting M, Boreham A, Brodwolf R, Vávrová K, Alexiev U, Friess W, Hedtrich S. 2015. Interactions of hyaluronic acid with the skin and implications for the dermal delivery of biomacromolecules. Mol Pharm 12:1391–1401. https://doi.org/10.1021/mp500676e.
38. Vyumvuhore R, Tfayli A, Duplan H, Delalleau A, Manfait M, Baillet-Guffroy A. 2013. Effects of atmospheric relative humidity on stratum corneum structure at the molecular level: ex vivo Raman spectroscopy analysis. Analyst 138:4103. https://doi.org/10.1039/c3an00716b.
39. Imokawa G, Kuno H, Kawai M. 1991. Stratum corneum lipids serve as a bound-water modulator. J Invest Dermatol 96:845–851. https://doi.org/10.1111/1523-1747.ep12474562.
40. Vyumvuhore R, Tfayli A, Biniek K, Duplan H, Delalleau A, Manfait M, Dauskardt R, Baillet-Guffroy A. 2015. The relationship between water loss, mechanical stress, and molecular structure of human stratum corneum ex vivo. J Biophotonics 8:217–225. https://doi.org/10.1002/jbio.201300169.
41. Park AC. 1972. Rheology of stratum corneum-II: a physico-chemical investigation of factors influencing the water content of the corneum. J Soc Cosmet 23:13–21.
42. Leveque JL, Escoubez M, Rasseneur L. 1987. Water-keratin interaction in human stratum corneum. Bioeng Ski 3:227–242.
43. Yamamura T, Tezuka T. 1989. The water-holding capacity of the stratum corneum measured by 1 H-NMR. J Invest Dermatol 93:160–164. https://doi.org/10.1111/1523-1747.ep12277392.
44. Björklund S, Andersson JM, Pham QD, Nowacka A, Topgaard D, Sparr E. 2014. Stratum corneum molecular mobility in the presence of natural moisturizers. Soft Matter 10:4535–4546. https://doi.org/10.1039/c4sm00137k.
45. Van Duzee BF. 1978. The influence of water content, chemical treatment and temperature on the rheological properties of stratum corneum. J Invest Dermatol 71:140–144. https://doi.org/10.1111/1523-1747.ep12546836.
46. Choe C, Schleusener J, Lademann J, Darvin ME. 2017. Keratin-water-NMF interaction as a three layer model in the human stratum corneum using in vivo confocal Raman microscopy. 7:15900.
47. Nakagawa N, Sakai S, Matsumoto M, Yamada K, Nagano M, Yuki T, Sumida Y, Uchiwa H. 2004. Relationship between NMF (lactate and potassium) content and the physical properties of the stratum corneum in healthy subjects. J Invest Dermatol 122:755–763. https://doi.org/10.1111/j.0022-202X.2004.22317.x.
48. Sakai S, Yasuda R, Sayo T, Ishikawa O, Inoue S. 2000. Hyaluronan exists in the normal stratum corneum. J Invest Dermatol 114:1184–1187. https://doi.org/10.1046/j.1523-1747.2000.00992.x.
49. Maytin EV, Chung HH, Seetharaman VM. 2004. Hyaluronan participates in the epidermal response to disruption of the permeability barrier in vivo. Am J Pathol 165:1331–1341. https://doi.org/10.1016/S0002-9440(10)63391-3.
50. Raab S, Yatskayer M, Lynch S, Manco M, Oresajo C. 2017. Clinical evaluation of a multi-modal facial serum that addresses hyaluronic acid levels in skin. J Drugs Dermatology 16:884–890.
51. Caussin J, Gooris GS, Janssens M, Bouwstra JA. 2008. Lipid organization in human and porcine stratum corneum differs widely, while lipid mixtures with porcine ceramides model human stratum corneum lipid organization very closely. Biochim Biophys Acta 1778:1472–1482. https://doi.org/10.1016/j.bbamem.2008.03.003.
52. Abrams K, Harvell JD, Shriner D, Wertz P, Maibach H, Maibach HI, Rehfeld SJ. 1993. Effect of organic solvents on in vitro human skin water barrier function. J Invest Dermatol 101:609–613. https://doi.org/10.1111/1523-1747.ep12366068.
53. Lampe MA, Burlingame AL, Whitney J, Williams ML, Brown BE, Roitman E, Elias PM. 1983. Human stratum corneum lipids: characterization and regional variations. J Lipid Res 24:120–130. https://doi.org/10.1016/S0022-2275(20)38005-6.
54. Wertz PW, Kremer M, Squier CA. 1992. Comparison of lipids from epidermal and palatal stratum corneum. J Invest Dermatol 98:375–378. https://doi.org/10.1111/1523-1747.ep12499809.

55. Bligh EG, Dyer WJ. 1959. A rapid method of total lipid extraction and purification. Can J Biochem Physiol 37:911–917. https://doi.org/10.1139/o59-099.
56. Bow JR, Sonoki Y, Uchiyama M, Shimizu E, Tanaka K, Dauskardt RH. 2020. Lipid loss increases stratum corneum stress and drying rates. Skin Pharmacol Physiol 33:180–188. https://doi.org/10.1159/000507456.
57. Robinson M, Visscher M, Laruffa A, Wickett R. 2010. Natural moisturizing factors (NMF) in the stratum corneum (SC). I. Effects of lipid extraction and soaking. J Cosmet Sci 61:13–22.
58. Jokura Y, Ishikawa S, Tokuda H, Imokawa G. 1995. Molecular analysis of elastic properties of the stratum corneum by solid-state 13 C-nuclear magnetic resonance spectroscopy. J Invest Dermatol 104:806–812. https://doi.org/10.1111/1523-1747.ep12607005.
59. Wertz PW, Swartzendruber DC, Kitko DJ, Madison KC, Downing DT. 1989. The role of the corneocyte lipid envelopes in cohesion of the stratum corneum. J Invest Dermatol 93:169–172. https://doi.org/10.1111/1523-1747.ep12277394.
60. Ohnishi Y, Okino N, Ito M, Imayama S. 1999. Ceramidase activity in bacterial skin flora as a possible cause of ceramide deficiency in atopic dermatitis. Clin Diagn Lab Immunol 6:101–104. https://doi.org/10.1128/CDLI.6.1.101-104.1999.
61. Nath S, Kumari N, Bandyopadhyay D, Sinha N, Majumder PP, Mitra R, Mukherjee S. 2020. Dysbiotic lesional microbiome with filaggrin missense variants associate with atopic dermatitis in India. Front Cell Infect Microbiol 10:570423. https://doi.org/10.3389/fcimb.2020.570423.
62. Williams MR, Nakatsuji T, Sanford JA, Vrbanac AF, Gallo RL. 2017. Staphylococcus aureus induces increased serine protease activity in keratinocytes. J Invest Dermatol 137:377–384. https://doi.org/10.1016/j.jid.2016.10.008.
63. Patti JM, Schneider A, Garza N, Boles JO. 1995. Isolation and characterization of pcp, a gene encoding a pyrrolidone carboxyl peptidase in Staphylococcus aureus. Gene 166:95–99. https://doi.org/10.1016/0378-1119(95)00561-0.
64. Yang JJ, Chang TW, Jiang Y, Kao HJ, Chiou BH, Kao MS, Huang CM. 2018. Commensal staphylococcus aureus provokes immunity to protect against skin infection of methicillin-resistant staphylococcus aureus. Int J Mol Sci 19:1290. https://doi.org/10.3390/ijms19051290.
65. Zhou C, Bhinderwala F, Lehman MK, Thomas VC, Chaudhari SS, Yamada KJ, Foster KW, Powers R, Kielian T, Fey PD. 2019. Urease is an essential component of the acid response network of Staphylococcus aureus and is required for a persistent murine kidney infection. PLoS Pathog 15:e1007538. https://doi.org/10.1371/journal.ppat.1007538.
66. Ibberson CB, Jones CL, Singh S, Wise MC, Hart ME, Zurawski DV, Horswill AR. 2014. Staphylococcus aureus hyaluronidase is a CodY-regulated virulence factor. Infect Immun 82:4253–4264. https://doi.org/10.1128/IAI.01710-14.
67. Dapic I, Jakasa I, Yau NLH, Kezic S, Kammeyer A. 2013. Evaluation of an HPLC method for the determination of natural moisturizing factors in the human stratum corneum. Anal Lett 46:2133–2144. https://doi.org/10.1080/00032719.2013.789881.
68. Takahashi M, Kawasaki K, Tanaka M, Ohta S, Tsuda Y. 1981. The mechanism of stratum corneum plasticization with water, p 67–73. *In* Bioengineering and the skin. Springer, Dordrecht, Netherlands.
69. Mojumdar EH, Pham QD, Topgaard D, Sparr E. 2017. Skin hydration: interplay between molecular dynamics, structure and water uptake in the stratum corneum. Sci Rep 7. https://doi.org/10.1038/s41598-017-15921-5.
70. Arikawa J, Ishibashi M, Kawashima M, Takagi Y, Ichikawa Y, Imokawa G. 2002. Decreased levels of sphingosine, a natural antimicrobial agent, may be associated with vulnerability of the stratum corneum from patients with atopic dermatitis to colonization by Staphylococcus aureus. J Invest Dermatol 119:433–439. https://doi.org/10.1046/j.1523-1747.2002.01846.x.
71. Kong HH, Oh J, Deming C, Conlan S, Grice EA, Beatson MA, Nomicos E, Polley EC, Komarow HD, Murray PR, Turner ML, Segre JA, NISC Comparative Sequence Program. 2012. Temporal shifts in the skin microbiome associated with disease flares and treatment in children with atopic dermatitis. Genome Res 22:850–859. https://doi.org/10.1101/gr.131029.111.
72. Levin J, Friedlander SF, Del Rosso JQ. 2013. Atopic dermatitis and the stratum corneum part 2: other structural and functional characteristics of the stratum corneum barrier in atopic skin. J Clin Aesthet Dermatol 6:49–54.
73. Ananthapadmanabhan KP, Moore DJ, Subramanyan K, Misra M, Meyer F. 2004. Cleansing without compromise: the impact of cleansers on the skin barrier and the technology of mild cleansing. Dermatol Ther 17 Suppl 1:16–25. https://doi.org/10.1111/j.1396-0296.2004.04s1002.x.
74. Kirk JE. 1966. Hand washing. Quantitative studies on skin lipid removal by soaps and detergents based on 1500 experiments. Acta Derm Venereol Suppl (Stockh) 1–183.
75. Monteiro-Riviere NA. 2010. Toxicology of the skin. CRC Press, Boca Raton, FL.
76. Riethmuller C, McAleer MA, Koppes SA, Abdayem R, Franz J, Haftek M, Campbell LE, Maccallum SF, McLean WHI, Irvine AD, Kezic S. 2015. Filaggrin breakdown products determine corneocyte conformation in patients with atopic dermatitis. J Allergy Clin Immunol 136:1573–1580.32. https://doi.org/10.1016/j.jaci.2015.04.042.
77. Feuillie C, Vitry P, McAleer MA, Kezic S, Irvine AD, Geoghegan JA, Dufrêne YF. 2018. Adhesion of Staphylococcus aureus to corneocytes from atopic dermatitis patients is controlled by natural moisturizing factor levels. mBio 9. https://doi.org/10.1128/mBio.01184-18.
78. Kligman AM, Christophers E. 1963. Preparation of isolated sheets of human stratum corneum. Arch Dermatol 88:702–705. https://doi.org/10.1001/archderm.1963.01590240026005.
79. Warner RR, Boissy YL, Lilly NA, Spears MJ, McKillop K, Marshall JL, Stone KJ. 1999. Water disrupts stratum corneum lipid lamellae: damage is similar to surfactants1. J Invest Dermatol 113:960–966. https://doi.org/10.1046/j.1523-1747.1999.00774.x.
80. Dhandapani N, Samuelsson K, Sköld M, Zohrevand K, German GK. 2020. Mechanical, compositional, and microstructural changes caused by human skin maceration. Extrem Mech Lett 41:101017. https://doi.org/10.1016/j.eml.2020.101017.
81. Schaefer H, Rodelmeier TE. 1996. Skin barrier: principles of percutaneous absorption. Karger, Basel, Switzerland.
82. Anderson RL, Cassidy JM. 1973. Variations in physical dimensions and chemical composition of human stratum corneum. J Invest Dermatol 61:30–32. https://doi.org/10.1111/1523-1747.ep12674117.
83. Van Duzee BF. 1975. Thermal analysis of human stratum corneum. J Invest Dermatol 65:404–408. https://doi.org/10.1111/1523-1747.ep12607656.
84. Lipsky ZW, German GK. 2019. Ultraviolet light degrades the mechanical and structural properties of human stratum corneum. J Mech Behav Biomed Mater 100:614602. https://doi.org/10.1016/j.jmbbm.2019.103391.
85. Barnes TM, Greive KA. 2013. Use of bleach baths for the treatment of infected atopic eczema. Australas J Dermatol 54:251–258. https://doi.org/10.1111/ajd.12015.
86. Racioppi F, Daskaleros PA, Besbelli N, Borges A, Deraemaeker C, Magalini SI, Martinez AR, Pulce C, Ruggerone ML, Vlachos P. 1994. Household bleaches based on sodium hypochlorite: review of acute toxicology and poison control center experience. Food Chem Toxicol 32:845–861. https://doi.org/10.1016/0278-6915(94)90162-7.
87. Fisher RG, Chain RL, Hair PS, Cunnion KM. 2008. Hypochlorite killing of community-associated methicillin-resistant Staphylococcus aureus. Pediatr Infect Dis J 27:934–935. https://doi.org/10.1097/INF.0b013e318175d871.
88. Annaidh AN, Bruyère K, Destrade M, Gilchrist MD, Otténio M. 2012. Characterization of the anisotropic mechanical properties of excised human skin. J Mech Behav Biomed Mater 5:139–148. https://doi.org/10.1016/j.jmbbm.2011.08.016.